Combustion and Flame 237 (2022) 111719

Contents lists available at ScienceDirect

Combustion and Flame

journal homepage: www.elsevier.com/locate/combustflame

Natural gas versus methane: Ignition kinetics and detonation limit behavior in small tubes

Jackson Crane, Xian Shi*, Rui Xu[1], Hai Wang

Department of Mechanical Engineering, Stanford University, Stanford, CA 94305, USA

ARTICLE INFO

Article history:
Received 1 June 2021
Revised 25 August 2021
Accepted 26 August 2021

Keywords:
Natural gas detonation
Methane detonation
Detonation limit
Natural gas surrogate

ABSTRACT

Detonation properties of methane and natural gas were studied using ZND simulations and detonation limit experiments. The experiments were performed in two tube sizes, 32 mm and 6.4 mm in inner diameter over a range of initial pressures (between 3.4 kPa and 35 kPa) and with stoichiometric fuel-oxygen compositions. The fuels considered are high purity methane, high purity methane with dopant ozone, a real natural gas, and a family of natural gas surrogates. The natural gas surrogates were developed based on North American natural gas composition variations and designed to capture the expected mean and variance of fundamental combustion properties of natural gases. All natural gases tested in this work show a substantially smaller detonation induction length (about 40%) and lower detonation pressure limit (30% in terms of limiting pressure) than high purity methane. The ozonated methane at 3000 PPMv of ozone doping performed similarly to the natural gases. Overall, the results suggest that in methane-based mixtures, a smaller induction length correlates with a more predictable detonation behavior as evidenced by a lower detonation pressure limit. As such, natural gases are expected to have a wider operating range when used as a fuel for detonation-based engines. As importantly, induction length calculation results reveal that the variability in detonation and combustion behaviors resultant from composition variability is expected to be similar between natural gases and commercial methane. Finally, the results suggest that for safety-related studies, neat methane is a poor surrogate for studying natural gas explosions.

1. Introduction

Pressure-gain detonation combustors have attracted significant attention in recent years [1–3]. Of particular interest is the rotating detonation engine (RDE) in which an azimuthally propagating detonation wave is sustained to combust a fuel-oxidizer mixture. Potential fuels for these engines include hydrogen, methane or natural gas (NG), kerosene-based rocket fuels (e.g., RP-1), and kerosene-based jet fuels (e.g., Jet A and JP-8) [4]. In recent years, methane and liquefied natural gas have become emerging rocket fuels, as they are generally easier to handle than hydrogen, and have a higher specific impulse and a lower coking propensity compared to some of the kerosene-based fuels [5]. Natural gas is also currently a preferred option for stationary power generation due to its availability, low cost, and the existing infrastructure [6]. For these reasons, methane or natural gas high-pressure combustion and detonation have been intensely studied in the past few years [7–14]. Demonstrations of methane or natural gas fueled RDEs have proved the viability of such fuels.

Understanding and predicting the detonation behavior of natural gas is also of critical importance for preventing accidents associated with its storage, handling, and utilization (see, e.g., [15–17]). Natural gas explosions in coal mines were responsible for hundreds of fatalities in the US alone over the past few decades [18]. Although most explosion accidents in mines are deflagrations, detonations are a worst-case accident scenario which must be understood and avoided [19]. Recent studies on detonation explosion safety have focused on deflagration-to-detonation transition dynamics in methane and natural gas [19–21], and detonation cellular structure [22] and propagation limits [23] of methane-based mixtures.

To date, little to no experimental insight is available about the difference between the detonation properties of methane and natural gas. It is often assumed that the combustion properties between these fuels are similar or even identical. Very high purity methane (>99.9%) is often the fuel of choice for academic studies because a neat fuel is perceived as the more convenient

* Corresponding author.
E-mail address: xianshi@stanford.edu (X. Shi).
[1] Current address: Department of Chemistry, Stanford University, Stanford, CA 94305, USA

https://doi.org/10.1016/j.combustflame.2021.111719
0010-2180/

Table 1
Molar percentage (%) range of major and minor components in typical North American natural gases (NGs) (values taken from [29]).

Species	North American NGs
Methane (CH_4)	87.0–96.0
Ethane (C_2H_6)	1.8–5.1
Propane (C_3H_8)	0.1–1.5
iso-Butane (i-C_4H_{10})	0.01–0.3
n-Butane (n-C_4H_{10})	0.01–0.3
iso-Pentane (i-C_5H_{12})	Trace–0.14
n-Pentane (n-C_5H_{12})	Trace–0.04
Hexanes plus (e.g. n-C_6H_{14})	Trace–0.06
Carbon Dioxide (CO_2)	0.1–1.0
Nitrogen (N_2)	1.3–5.6
Oxygen (O_2)	0.01–0.1
Hydrogen (H_2)	Trace–0.02

and repeatable option as compared to a multi-component mixture with potential composition variations. In many accident prevention studies, neat methane or a single representative natural gas is used to quantify the expected detonation behaviors [19–21]. While there has been a wealth of fundamental detonation studies on methane [24–27], the impact of the minor species in natural gas on its detonation properties was rarely addressed. Only one study suggested that different natural gases may have differing detonation properties based on one-dimensional detonation calculations [28], and yet no experimental work has been done to quantify the effect of natural gas variability on detonation.

Natural gas composition can vary seasonally and by location. In this work we focus on North American natural gases. Typical species compositions of North American natural gas are shown in Table 1, as specified by the North American Energy Standard Board (NAESB) [29]. Evident is the wide variability in minor species concentrations. Our previous work has shown that even dopant concentrations of some species (e.g., ozone) can change detonation structure and limits by a wide margin [30,31].

In addition to the composition variability of natural gases, commercial-grade methane can have appreciable variability that may result in a notable impact on the detonation properties. High purity methane (i.e., >99.0%) is likely prohibitively expensive for most practical energy conversion applications, in which case a commercial-grade methane is typically used instead. Commercial 1.3-grade methane has a purity of ≥93.0% methane [32]. This purity is, in fact, comparable to many of the natural gases.

The present work aims to examine and compare detonation behaviors of methane and natural gases with varying compositions both numerically and experimentally. We study (a) high-purity methane which is often used in research and laboratory settings, (b) natural gases of compositions typically found in North American pipelines, and (c) commercial-grade methane which is compositionally in between high-purity methane and typical natural gases. The specific goals of this study are threefold: (1) to compare the average detonation performance of methane and natural gas, (2) to quantify the effect of composition variability on the detonation performance of methane and natural gas, and (3) to provide a practical solution for working with natural gas for laboratory and computational studies. To achieve the last goal, we propose a set of composition surrogates for North American natural gases, including a nominal surrogate, and four surrogates which capture the composition variability of natural gases. The findings of this study are expected to inform fuel choices (methane versus natural gas) for engine designers, to shed light on the suitability of using methane as a surrogate of natural gas in detonation studies, and to quantify expected variability from different fuels.

We conducted three sets of tests: (1) fundamental combustion property calculations (i.e., ignition delay time, laminar flame speed, extinction residence time in perfectly stirred reactors) for surrogate development, (2) one-dimensional Zel'dovich–von Neumann–Döring (ZND) detonation simulations, and (3) experimental detonation velocity deficit and limit measurements. For the fundamental combustion property and ZND calculations, a Monte Carlo (MC) sampling approach is used to account for typical natural gas and commercial methane composition variations. Fundamental combustion property calculations are useful because they approximate a range of real combustion scenarios, while ZND simulations are useful because the ZND-based induction length (Δ_i) is shown to directly correlate with structural features and properties of detonation waves [30,31,33–36]. Both sets of calculations are computationally tractable as far as MC simulations are concerned. Experimentally, we are interested in detonation limit behavior in small tubes as a proxy for examining the variation of detonation behaviors due to the fuel choice and fuel composition variability. A detonation wave with insufficient or slow heat release cannot successfully propagate at the theoretical Chapman-Jouguet (CJ) velocity in a narrow channel or tube due to the various loss mechanisms [33]. We quantify the detonation limit behavior by measuring the velocity deficit, i.e., the difference between the actual detonation propagation velocity in practical geometries and the theoretical CJ speed for a given mixture and condition.

Table 2
Molar percentage (%) of the Boise natural gas sample (measured by gas chromatography).

Species	Boise sample
Methane (CH_4)	92.05
Ethane (C_2H_6)	6.20
Propane (C_3H_8)	0.70
iso-Butane (i-C_4H_{10})	Trace
n-Butane (n-C_4H_{10})	Trace
Carbon Dioxide (CO_2)	1.05

2. Numerical and experimental methods

2.1. Tested mixtures

Several fuels were considered in the present study (with oxygen as the oxidizer): (1) methane (Ultra High Purity, Grade 3.7, Purity ≥99.97%), (2) ozonated methane (3000 PPMv ozone added to the methane-oxygen mixture), (3) the natural gas surrogates developed in Section 3.1, (4) a real natural gas. The ozonated methane tests were designed to illustrate the direct link between reaction kinetics and detonation properties in methane-based mixtures. Earlier work has shown that ozone as an additive at dopant levels can control the induction length of hydrogen-oxygen mixtures and does not affect other relevant properties (e.g., thermodynamic properties, wave speed, and heat release) [30]. Such a link is useful to shed mechanistic insight for studying natural gas detonation, specifically to what extent the composition variability impacts the repeatability of natural gas detonation in laboratory and in practical applications. The real natural gas sample was sourced from Boise, Idaho [37], and the composition of this sample was measured by gas chromatography [14], and is reported in Table 2. Note that the mole fraction of ethane in the Boise sample is higher than the upper range of typical North American gases. As a mild outlier of North American natural gas, the Boise sample was chosen to demonstrate whether composition outliers are well-captured by the statistical surrogate approach proposed in the present work.

2.2. Fundamental combustion property simulations

As mentioned earlier, the natural gas surrogates were developed to capture the mean and variance of typical North American natural gases. To evaluate the nominal properties and variability

of typical natural gases, a Monte Carlo sampling was employed. About 100 random samples of natural gases are considered, with the mole fraction of each constituent species (except for CH_4) randomly sampled within the prescribed ranges shown in Table 1 assuming a uniform probability distribution. After sampling, the remainder of the mixture is set to be CH_4. Fundamental combustion properties, namely ignition delay time, laminar flame speed, and perfectly stirred reactor (PSR) extinction residence time, were calculated for each Monte Carlo sample in support of the surrogate development. For ignition delay time, four T_5 temperatures (i.e., the post-reflected-shock temperature in a shock tube ignition delay experiment) were considered: 1100 K, 1200 K, 1300 K, and 1400 K. Laminar flame speed calculations were performed at unburned gas temperature $T_u = 298$ K and PSR extinction calculations at inlet temperature $T_{inl} = 700$ K. Ignition delay time, laminar flame speed, and PSR extinction calculations were all performed at an initial pressure of $p = 60$ atm in oxygen at an equivalence ratio of unity. These thermodynamic conditions were chosen because they are relevant to both detonation and also rocket combustion conditions.

The fundamental combustion property simulations were carried out using the Foundational Fuel Chemistry Model Development Version Y (FFCM-Y) [38], which is an expanded version of Foundational Fuel Chemistry Model Version 1.0 (FFCM-1) [39]. It describes the combustion chemistry of small hydrocarbon fuels (H_2/CO/C_1-C_4) using up-to-date kinetic knowledge. Additionally, the chemistry of minor C_5 and C_6 alkane species (see, Table 1) was added into the FFCM-Y model from the reaction models of JetSurF 2.0 [40] and Lawrence Livermore National Laboratory [41]. FFCM-2 (soon to be released), the fully optimized version of FFCM-Y, does not differ substantially from FFCM-Y for predicting methane combustion.

Computations of ignition delay times, laminar flame speeds, and PSR extinction residence times were performed in CHEMKIN [42]. The ignition delay time was computed using the SENKIN package [43]. The onset of ignition was defined as the time reaching the maximum derivative of pressure with respect to time under constant volume and adiabatic assumptions. The PSR extinction residence time were determined through calculating the *S*-curve using the PSR package [44] under constant pressure and adiabatic assumption. The extinction time was defined as the reaction time corresponding to the upper turning point of the *S*-curve. Laminar flame speed was computed using PREMIX [45] with multicomponent transport and thermal diffusion.

2.3. ZND simulations

Steady one-dimensional ZND calculations were performed for each fuel studied over a range of initial pressures which we examined experimentally, i.e., 3 to 35 kPa, at 295 K. The high purity methane (≥99.97% CH_4) is approximated as neat methane (100% CH_4) in the simulations. The oxidizer in all simulated and experimental cases was oxygen at the corresponding stoichiometric equivalence ratio. The numerical solver used in all ZND cases is a modified form of the Caltech SD Toolbox [46] for MATLAB using Cantera [47]. FFCM-Y (described above) with the Princeton ozone sub-model [48] was used as the kinetic model for all ZND calculations.

Monte Carlo ZND calculations were also performed to evaluate the impact of composition variation of methane and natural gas on expected detonation behaviors. Two MC ZND sampling techniques were employed. The first technique (denoted henceforth as sampling plan 1) is a parallel to the surrogate development sampling plan, and considers 100 random samples of natural gases with the mole fraction of each constituent species (except for CH_4) randomly sampled within the prescribed ranges shown in Table 1 assuming a uniform probability distribution. After sampling, the remainder of the mixture is set to be CH_4. Sampling plan 1 is used to validate the suitability of the fundamental combustion calculations used for surrogate development for detonation conditions.

Table 3
Monte Carlo sampling of commercial methane and natural gas compositions. X_i denotes the mole fraction of the ith fuel species considered, S_i denotes the name of the ith fuel species, and $n = 12$ is the total number of fuel species as listed in Table 1.

Sampling plan	X_{CH_4} (%)	Samples
1	$100 - \sum_{i=1, S_i \neq CH_4}^{n} X_i$	100
2	80	100
	85	100
	90	100
	95	100
	97.5	100
	99	100

The second technique (denoted henceforth as sampling plan 2) prescribes a mole fraction of methane (values of 0.80, 0.85, 0.90, 0.95, 0.975, 0.99 are chosen) and the remaining component mole fractions are first sampled from a uniform distribution with the ranges shown in Table 1 and then renormalized to the remaining mole fraction. One hundred samples for each mole fraction of methane are considered. Sampling plan 2 seeks to examine the potential variability which could exist in commercial methane, and also explore the effect of varying methane concentration in natural gases.

A summary of the MC simulation conditions is shown in Table 3. One hundred ZND simulations are performed for each sampled composition (100 simulations for sampling plan 1 and 600 simulations for sampling plan 2). The initial pressure was set to 25 kPa and the initial temperature remained at 295 K. The average and standard deviation of both induction length and Chapman-Jouguet (CJ) velocity were recorded, and the profiles with the closest values to the statistical induction lengths are presented (in this case the mean and $\pm 2\sigma$). The induction length is defined here as the distance between the leading shock wave and the maximum temperature gradient [46]. It captures the length scale associated with the ignition behind the shock wave.

2.4. Experimental measurements

Detonation limit experiments were conducted in a linear detonation apparatus consisting of a 1.2 m long stainless-steel driver section with an inner diameter (ID) of 73 mm, and a 2.4 m long test section. Two polycarbonate test sections were used, one 32 mm in ID and the other 6.4 mm. A schematic of the apparatus is shown in Fig. 1. Besides the high-purity methane, the ozonated methane, and the Boise natural gas, three surrogate natural gases were prepared and tested: the nominal surrogate, the 2σ 'fast' surrogate, and the 2σ 'slow' surrogate developed in Section 3.1. The gases used to form the natural gas surrogate samples were ethane (Chemically Pure grade 2.0, Purity ≥99.0%), propane (Instrument grade 2.5, Purity ≥99.5%), nitrogen (Research grade 5.0, Purity ≥99.999%), and carbon dioxide (Instrument grade 2.5, Purity ≥99.5%). All experiments were performed at a stoichiometric equivalence ratio in oxygen (Grade 2.6, Purity ≥99.6%).

Mixtures were prepared using sonic nozzles with ozone generated, when applicable, using an inline corona discharge ozone generator fed with oxygen. In the case of the surrogate natural gases, a tank of the minor components (ethane, propane, nitrogen, carbon dioxide in the appropriate relative fraction for each surrogate) was prepared using the partial pressure technique. The minor components were then blended with methane and oxygen with sonic nozzles upon filling. Mixtures were ignited within 30 seconds

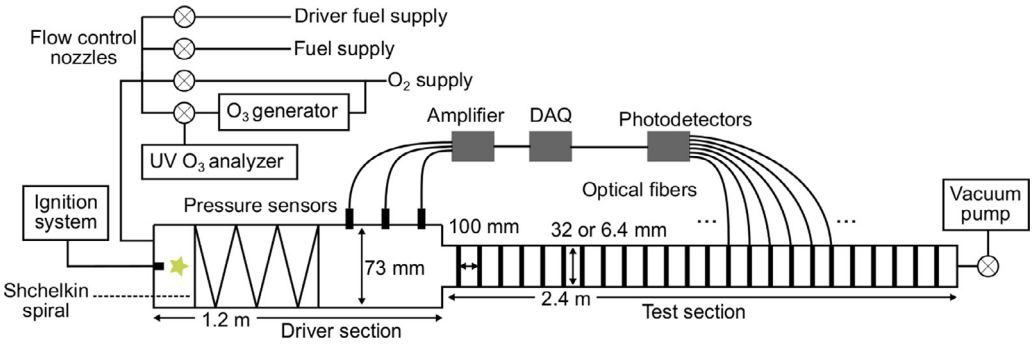

Fig. 1. Schematic of the linear detonation apparatus.

of filling, designed to minimize any pre-shock ozone decomposition. The driver section is outfitted with a Shchelkin spiral approximately 0.5 m in length to aid the deflagration-to-detonation transition. A range of sub-atmospheric pressures (3–35 kPa) were tested to vary the reactivity of the mixtures and evaluate the detonation limits. These pressures were chosen because of their experimental accessibility, but the trends among different fuels are expected to be similar at higher pressures characteristic of engine and accident conditions, where detonation limits are relevant due to geometric confinement and fuel-lean or fuel-rich compositions. A comparison between calculated induction lengths of methane and natural gas mixtures at various pressures and compositions is provided in the supplementary materials (SMM). In this study, for near-limit and the limit conditions (e.g., those at lower pressures), a small amount of a more reactive mixture (a stoichiometric ethylene-oxygen mixture), was used in the driver section to assist detonation initiation. Detonation velocity deficits were calculated based on the time-of-arrival of the detonation front, recorded by 24 digital photodetectors coupled to optical fibers. Three pressure sensors were used in the driver section to validate that a detonation was achieved in the driver. Cell size measurements were made for the Boise natural gas or the ozonated methane using the soot foil technique at 4 pressures (10, 15, 20, 25 kPa) in the 32 mm ID test section. A more detailed description of the experimental apparatus and procedure can be found in [30,31].

Three fuels (methane, ozonated methane, and the Boise natural gas) were tested in both tube sizes (32 mm and 6.4 mm). These tests are designed to examine the role of kinetics in detonation limit behavior, and how a typical natural gas performs relative to methane. Two tube sizes were used for these tests to examine how the detonation limit differs in different sized geometries, specifically in relation to the reaction kinetics. The surrogate fuels were tested only in the 32 mm tube. These tests were designed to test the natural gas surrogate approach. Experiments in the 32 mm tube are sufficient for verifying the suitability of the surrogates experimentally, and for measuring the impact of composition variability on detonation limiting behavior compared to the other fuels tested.

3. Results and discussion

3.1. Natural gas surrogates

To provide a solution for working with natural gases, we propose a surrogate approach with the goal to capture both the expected mean combustion property values and their variabilities among North American natural gases (see Table 1). In developing the surrogates, we consider ignition delay time, laminar flame speed, and perfectly stirred reactor (PSR) extinction residence time. We consider these fundamental combustion properties so that the surrogates will not only be useful for detonation, but also for other combustion-related studies and applications. We note that ignition delay time at elevated temperatures is strongly correlated with ZND induction length, and so these fundamental combustion properties are expected to be relevant to detonation conditions. This is confirmed in Section 3.2.

Table 4
Mole fractions (%) of the five components in the natural gas surrogates.

Species	2σ slow	1σ slow	Mean	1σ fast	2σ fast
CH_4	91.2	91.2	91.2	91.2	91.2
C_2H_6	2.6	3.1	3.7	4.6	5.6
C_3H_8	0.4	0.7	0.8	1.2	1.7
N_2	5.0	4.3	3.7	2.6	1.4
CO_2	0.8	0.7	0.6	0.4	0.1

The computed distributions of ignition delay times are shown in Fig. 2, and the distributions of laminar flame speed and PSR extinction times are plotted in Fig. S2 of the SMM. All calculations of the fundamental properties were performed based on MC sampling plan 1 for North American natural gas in stoichiometric oxygen at initial (or constant) pressure of 60 atm and various initial (or unburned) temperatures. Our simulations show that within the thermodynamic conditions tested, all fundamental combustion properties of North American natural gas samples are well-bounded. As seen from Fig. 2, the 2σ values of ignition delay times are around 20% of the mean values. Meanwhile, the 2σ bounds of laminar flame speeds and PSR extinction residence times are found to be substantially smaller (~2% and ~3%, respectively; see Fig. S2). Overall, the MC simulation results show that laminar flame speeds and PSR extinction residence times are not significantly affected by the composition variations. While ignition time scales vary somewhat more, they are generally comparable or smaller than the known uncertainties of shock tube measurements of ignition delay. As such, we targeted the ignition delay as the key measure for the proposed North American natural gas surrogates.

In order to adequately match the combustion properties from the MC simulations, the surrogates are chosen to contain five (one major and four minor) components of natural gas, specifically methane, ethane, propane, nitrogen, and carbon dioxide. The methane mole fraction is fixed at 91.2%, the average of the North American natural gases, for all surrogates. The surrogate compositions are shown in Table 4. Five surrogate compositions are proposed here, representing the mean ignition characteristics of North American natural gases, along with the $\pm 2\sigma$ and $\pm 1\sigma$ in ignition delay times of North American natural gas statistically sampled. For example, the 2σ 'fast' surrogate composition has an ignition delay time of 2 standard deviation below the mean ignition delay time value. The criteria for the choice of surrogate compositions are described as follows. For the five surrogate components,

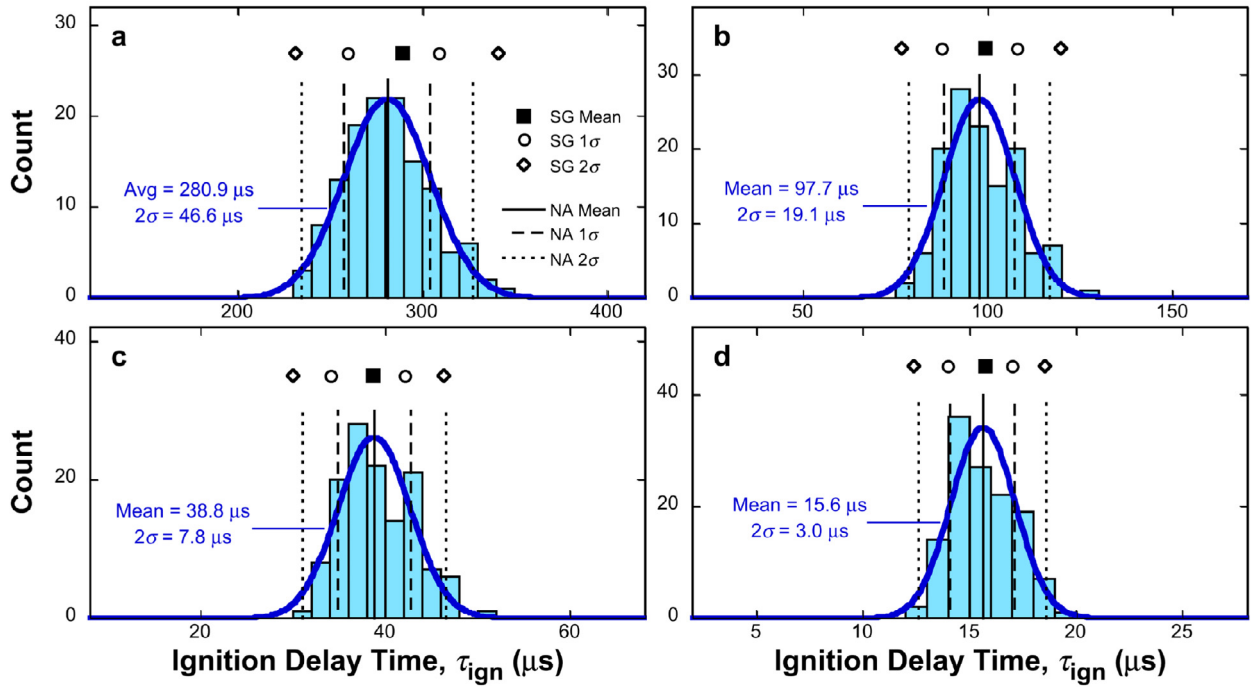

Fig. 2. Distributions of ignition delay times computed based on MC sampling plan 1 for North American (NA) natural gas in stoichiometric oxygen at p_5 = 60 atm, and T_5 = 1100 K **a**, 1200 K **b**, 1300 K **c**, and 1400 K **d**. The distributions are fitted to Gaussian curves which are shown to guide the eye. Also shown are the means of distributions (solid vertical lines), as well as the 1σ (dashed vertical lines) and 2σ (dotted vertical lines) bounds. The computed ignition delay times of the natural gas surrogates (SG) are displayed as symbols: mean (filled squares), 1σ fast and slow (open circles), and 2σ fast and slow (open diamonds). Note that the *y*-axes only serve for the histograms and fitted Gaussian curves.

their composition variations are considered as uniform distributions $U(a, b)$ where a and b are their upper and lower bounds shown in Table 1. The mole fraction X_i for each component i is initially determined by the choice of λ, such that $X_i = a_i + \lambda_i(b_i - a_i)$. For instance, in the mean surrogate, the λ values for all the five components are chosen to be 0.5, the average mole fractions; in the 2σ 'fast' surrogate, the λ value is set to be 1 for ethane and propane representing their composition upper bounds, and 0 for nitrogen and carbon dioxide as their composition lower bounds. The λ values for all the five components in the natural gas surrogates are also included in Table S1 of the SMM. Lastly, the mole fractions of the four minor components are scaled to fill the 8.8% of total composition excluding the mole fraction of methane (91.2%).

The performance of the natural gas surrogates in terms of ignition characteristics are tested and shown in Fig. 2. The computed ignition delay times of five surrogates (symbols) are compared with the mean and standard deviation bounds of the North American natural gas distributions (vertical lines). Clearly, over the range of test conditions, the natural gas surrogates capture the mean and variance of the ignition delay characteristics of North American natural gases very well. Additionally, the natural gas surrogates are also tested, as shown in Fig. S2, against laminar flame speed and PSR extinction residence times, even though the surrogate development was not based on these two combustion properties. Within the narrow variation bands of laminar flame speed and PSR extinction times, the natural gas surrogates are also able to capture their mean and variances reasonably well.

3.2. ZND calculation results

To test that the fundamental combustion properties used to develop the surrogates are applicable to detonation, ZND calculations were performed for the surrogate compositions. Figure 3 shows the temperature (T) as a function of distance behind the shock front (x) for mean (dash-dot line) and ±2σ (the shaded bands) surrogates. Also shown in Fig. 3 is the probability distribution function of induction length for ZND MC sampling plan 1. Although the natural gas surrogates were developed using ignition delay time and not ZND induction length, the surrogates describes the distribution in induction length resultant from the MC calculations well. For example, the surrogate compositions have induction lengths of 0.89 mm (mean), 0.69 mm (2σ fast) and 1.1 mm (2σ slow), as compared to inductions lengths from the MC sampling plan of 0.84 mm (mean), 0.70 mm (2σ fast) and 0.97 mm (2σ slow).

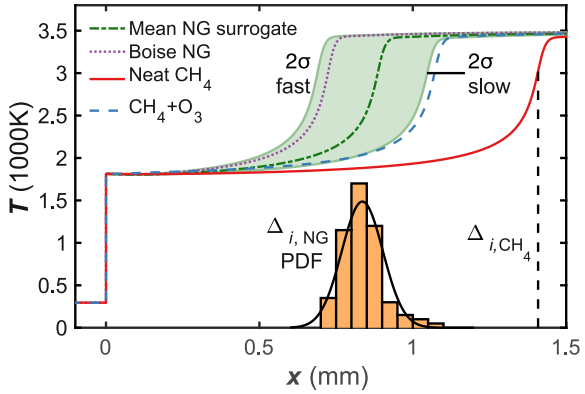

Fig. 3. ZND temperature profiles for stoichiometric neat methane (solid line), ozonated (3000 PPMv) methane (dashed line) and Boise natural gas (dotted line) at 25 kPa initial pressure in oxygen as well as the mean (dash-dotted line) and 2σ fast and slow surrogates (shaded bands). Annotated is the *x*-position of the induction length of neat methane (Δ_{i,CH_4}, dashed vertical line). Also shown is the probability distribution function (PDF) of natural gas induction length ($\Delta_{i,NG}$) based on MC sampling plan 1.

Also plotted in Fig. 3 are the ZND profiles of methane (solid line), ozonated methane (dashed line), and Boise natural gas (dotted line). Evident from the figure is the drastically longer induc-

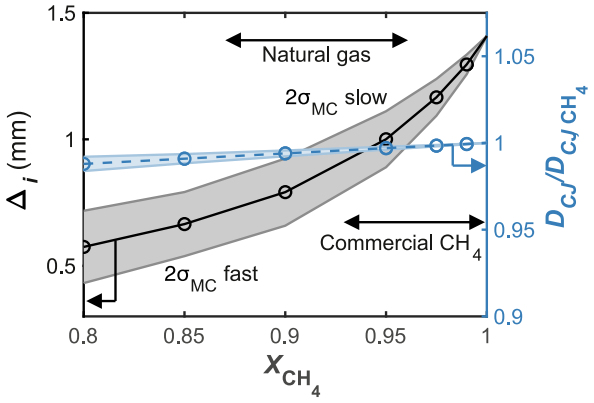

Fig. 4. Mean and $\pm 2\sigma_{MC}$ bands of ZND induction length (black line and grey bands, left y-axis) and mean and $\pm 2\sigma_{MC}$ bands of CJ velocity, normalized by CJ velocity of neat methane (blue dashed line and bands, right y-axis) as a function of methane mole fraction (Monte Carlo sampling plan 2). The ranges of methane mole fraction in commercial grade CH_4 ($X_{CH_4} \geq 0.93$) and North American natural gases ($0.87 \leq X_{CH_4} \leq 0.96$) are shown with arrows.

tion length of neat methane as compared to the ozonated methane and the Boise natural gas. Besides the difference in the induction length, the profiles are nearly identical in their total heat release, post-shock state, and equilibrium state. Although not shown, the CJ velocities of all mixtures are within 1% of one another. It follows then that any difference to be observed in limit behavior is due to differences in ignition time scales among the mixtures because their thermodynamic properties are close to identical.

To characterize the variability in detonation properties expected from natural gases, we first examine the ZND calculation results. As seen in the surrogate and Boise NG profiles in Fig. 3, the ZND profiles appear self-similar among all natural gases. Quantitatively the standard deviation in the induction length for MC sampling plan 1 is about 8% of the mean value. Furthermore, despite the large value of ethane present in the Boise sample, its ZND profile falls within the 2σ bands of the surrogate natural gas predictions.

The results from MC sampling plan 2 are shown in Fig. 4. The first observation is that the CJ speed (dashed line and shaded band) changes little with decreasing methane mole fraction; at most CJ speed is 2% lower when $X_{CH_4} = 0.8$ as compared to neat methane. There is also very little variability in CJ speed across the composition variations for any methane fraction (with $2\sigma_{MC}$ bands less than 0.5% for a given methane mole fraction). Induction length, however, decreases significantly with decreasing methane mole fraction, with the smallest observed induction length more than a factor of 3 smaller than that for neat methane. Across the range of compositions expected for commercial methane ($X_{CH_4} \geq 0.93$), we see a relatively large change in induction length, with induction length decreasing rapidly from neat methane. Meanwhile, across the somewhat wider expected methane concentrations of natural gas, the induction length changes slower. In terms of detonation properties, therefore, we expect that the variability of natural gas is similar to the variability of commercial methane, despite the wider composition variability of natural gas. Quantitatively, the $2\sigma_{MC}$ band of the expected induction lengths is approximately $\pm 30\%$ of the mean for both fuels. Due to the reduced induction length in natural gas, we expect that natural gas will have more reactive detonation properties than neat methane.

3.3. Detonation limit experiments

Typical signals from the pressure sensors and digital photodetectors are shown in Fig. 5a. The condition for this test is an ozonated methane-oxygen mixture at an initial pressure of 35 kPa

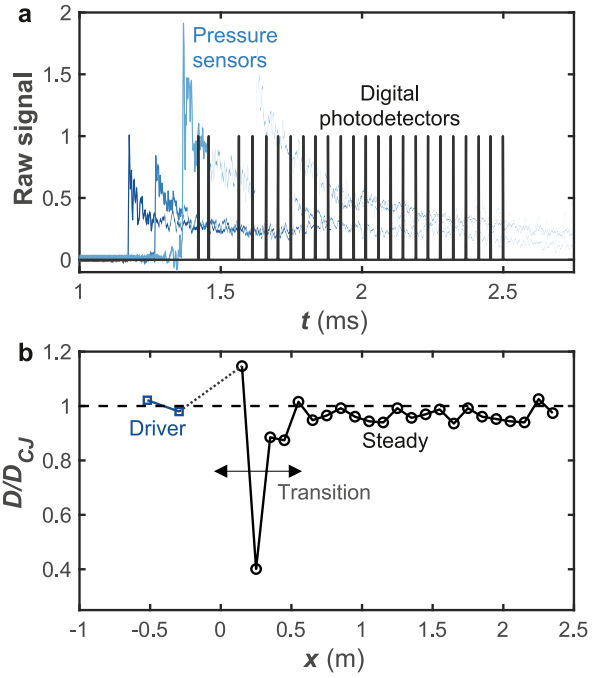

Fig. 5. Raw signal from a representative test (35 kPa, room temperature ozonated methane in the 6.4 mm test section), **a**. Blue (first three) signals are from the pressure sensors and grey signals are from the digital photodetectors. Velocity along the length of the apparatus from time of arrival measurements, **b**. Velocity measurements in the driver section from pressure signals are shown as blue squares, measurements in the test sections from the photodetectors are shown as black circles. The transition and steady regions in the test section are annotated.

and room temperature in the 6.4 mm tube. From the time of arrival of the pressure wave and digital photodetector signals, and their known physical spacing, a detonation velocity can be determined, as shown in Fig. 5b. The raw data in the figure demonstrate a sequence of events: (1) an initial detonation is established in the driver, (2) an entrance transition as the detonation exits the driver and reestablishes in the test section, and (3) a steady-velocity propagation in the bulk of the test section. The remainder of the plots and analysis focuses only on the propagation in the test section which did not appear to be affected by any entrance transition effects.

Detonations in the two test sections (32 mm and 6.4 mm IDs) exhibit different limit phenomena. Plotted in Fig. 6 are normalized velocities (by their respective CJ velocities) as a function of distance in the test section for the high purity methane, the ozonated methane, and the Boise NG at several chosen initial pressures as shown for both test section sizes. Generally, all of the mixtures exhibit similar qualitative features in the respective test sections. Although not shown, the surrogate NGs also display similar qualitative behaviors to the other mixtures in the 32 mm ID test section.

Detonations in the 32 mm ID tube generally propagate near the CJ velocity with some occurrence of oscillation even under pressures far above the detonation limit pressures of the respective mixtures. With a decreased initial pressure, velocity deficit becomes evident, until a critical pressure is reached (e.g., 5.2 kPa for high purity methane), where failure occurs as evidenced by the large velocity fluctuation and decay along the test section. For example, for the ozonated methane mixture, a small difference in pressure can result in the transition from a steady detonation to a failed detonation (i.e., the 5 kPa vs. the 4.6 kPa profile shown in Fig. 6b).

Detonations in the 6.4 mm ID tube, on the other hand, exhibit behaviors notably different from those in the 32 mm ID tube. All

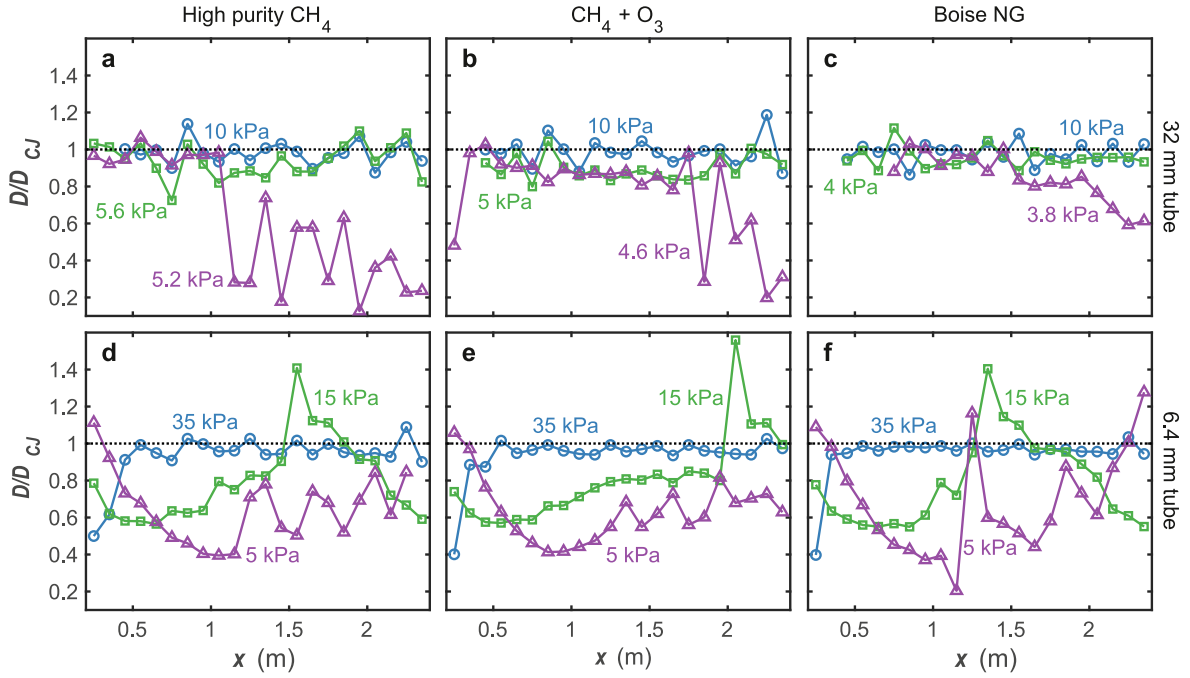

Fig. 6. Normalized velocity measured for three representative tests for each mixture and test section diameter combinations. Left panels: high purity methane; center panels: high-purity methane with 3000 PPMv ozone doping; right panels: Boise natural gas. Top row: tests in the 32 mm ID test section; bottom row: tests in the 6.4 mm ID test section.

mixtures show steady near-CJ velocities at 35 kPa with normalized velocities varying between 0.93 and 0.97 (Fig. 6d–f). As the initial pressure is decreased a second mode is observed, as shown by the velocity profiles measured at 15 kPa, where strong oscillations occur: the detonations cyclically become strongly overdriven then return to an underdriven state. Such detonation has been observed in previous work, particularly in experiments with much longer test section lengths [49], which allowed for observations over many cycles of this behavior. Although the test section in the present work is too short to determine the frequency of detonation oscillation, the nature of oscillation observed here is similar to previous observations. The final detonation mode observed in the 6.4 mm tube is a near-failure condition as observed at 5 kPa, wherein, after relaxing from the driver detonation, the wave propagates at a velocity well below the CJ velocity (approximately 0.6 times the CJ velocity) for the length of the test section. Neither of these more complex detonation modes are observed in the 32 mm test section. Suffice it to note that the observed strong dependence of detonation on tube size is in good agreement with past experimental studies [50,51].

To compare the detonation propagation behaviors, the velocity in the steady detonation region (when applicable) is averaged to provide a single average velocity for each pressure. To determine the magnitude of velocity fluctuation, a standard deviation of 100 point-to-point velocities, each of which is measured from a randomly sampled pair of time-of-arrival signals from the 24 photodetectors, is calculated. Figure 7 plots these averaged velocities and standard deviations as a function of pressure in the 32 mm test section, normalized by their respective CJ velocities. Selected error bars are shown; they represent one standard deviation of velocity fluctuations. Figure 7a shows the results for methane, ozonated methane, and the Boise NG sample, while Fig. 7b shows the results for three natural gas surrogates tested in the present work. As the pressure is decreased, all mixtures incur greater velocity deficits, until detonation eventually fails to propagate. The limiting behavior of the high purity methane is somewhat different from

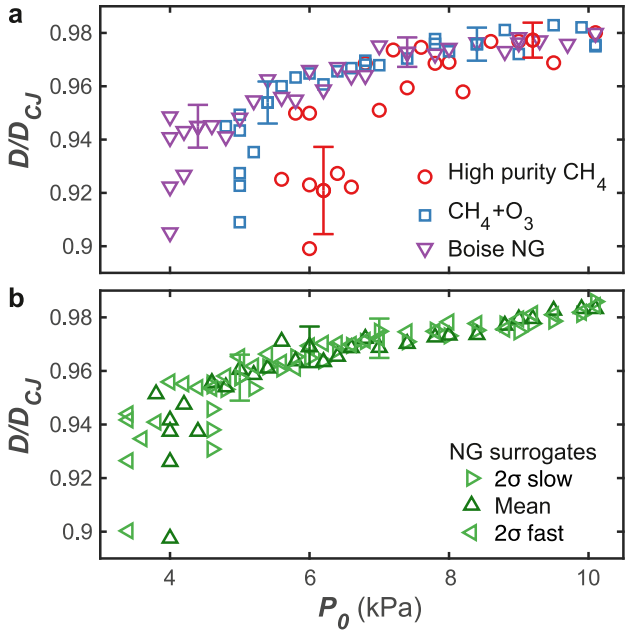

Fig. 7. Normalized velocity as a function of initial pressure in the 32 mm ID test section for high purity methane (circles), ozonated methane (squares), and a Boise natural gas (down-pointing triangles) **a**, and for three natural gas surrogates (2σ slow right-pointing triangles, mean up-pointing triangles, and 2σ fast left-pointing triangles) **b**. Error bars in both figures denote one standard deviation observed in wave velocity fluctuation.

the other mixtures: while the ozonated methane and natural gas exhibit a distinct limit with a sharp dropoff in velocity, the high purity methane shows a somewhat broader limit. In this broader limit (5.6 kPa to 6.4 kPa) a low normalized velocity (0.90 to 0.94) and large velocity fluctuations are observed. This difference in behavior between the mixtures may be due to the unstable detona-

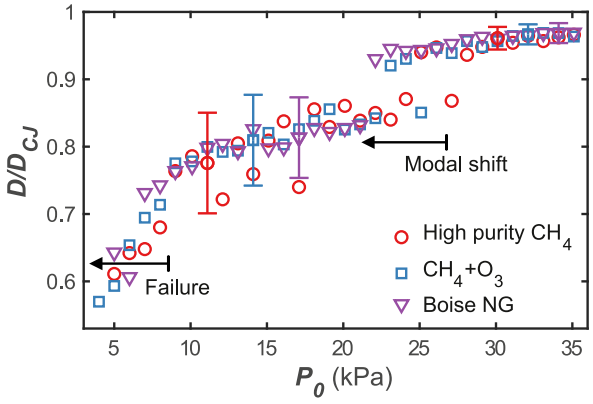

Fig. 8. Normalized averaged velocity as a function of initial pressure in the 6.4 mm ID test section for high purity methane (circles), ozonated methane (squares), and the Boise natural gas (down-pointing triangles). Annotated are the modal shift and failure regimes. Error bars denote one standard deviation in wave velocity fluctuation.

tion characteristics of neat methane, previously demonstrated in [52,53].

Clearly seen from Fig. 7a and b is that the different mixtures exhibit limits at different pressures. The high purity methane exhibits a detonation limit at the highest pressure (≈6 kPa), while the 2σ fast surrogate mixture shows the lowest limit at 3.4 kPa, a 40% decrease in limit pressure. The ozonated methane mixture (3000 PPMv ozone doping) exhibits a limit lower than that of methane. These observations clearly demonstrate the effect that reaction kinetics have on the detonation limit, as previously observed [31]. Furthermore, as suggested by their relative induction lengths (see Fig. 3), the Boise natural gas exhibits a lower pressure limit compared to the ozonated methane sample. The surrogates also exhibit the expected behavior, where the limit of the 2σ slow surrogate is at a higher pressure than the mean composition, and the 2σ fast surrogate has a lower pressure limit. None of the natural gas mixtures exhibit the less predictable behavior seen in the high purity methane. Finally, the natural gas surrogates show a relatively narrow band of limiting pressures, 4 ± 0.6 kPa, or a 30% variation across the 2σ surrogates.

Also observed in Fig. 7a and b is the very similar detonation velocity across all mixtures at higher pressures. This is entirely consistent with the observation from earlier work [31] that the velocity deficit away from the limit is determined largely by thermodynamics. As mentioned earlier, all major thermodynamic quantities (CJ speed, equilibrium state, and post-shock state) are practically identical among all mixtures.

The velocity data from the three mixtures studied in the 6.4 mm ID tube are compiled into Fig. 8. As in Fig. 7 for the 32 mm ID tube, each point represents an average velocity along the test section for a single test, with error bars denoting one standard deviation in wave velocity fluctuations. For this tube, however, many different velocity modalities were observed, as shown in Fig. 6. The modal transition from a steady velocity to a highly oscillatory mode is visible from the discontinuity in the velocity observed in the 22–27 kPa pressure range, annotated in the figure as the 'modal shift', and also in the increase in the amplitude of wave fluctuation with decreasing pressure, as evidenced by the increased error bar size. This modal shift occurs at different pressures for different mixtures: methane experiences the shift at around 27 kPa, while the ozonated methane and natural gas at around 23 kPa. The modal shift can be considered the main detonation limit, because propagation after the shift is highly oscillatory and propagates at average velocities substantially lower than the CJ velocity. After the modal shift, decreasing pressure yields an increased velocity deficit, until a complete failure at lower pressures. The final failure point appears to be relatively insensitive to the reaction kinetics specific to a mixture; all three mixtures tested exhibit a final failure point at around 5 kPa. As in the 32 ID mm tube, the high purity methane exhibits a less predictable velocity behavior, as evidenced by the greater degree of scatter in the data.

It is more informative to view the same 6.4 mm ID test section source data as a probability distribution of individual velocity measurements as a function of pressure, as suggested in [49]. Local velocity probability distributions as a function of initial pressure is plotted in Fig. 9. The observed velocities are calculated from each pair of adjacent optical sensors and then separated into bins of 0.05 normalized velocity units. Each column in each panel in Fig. 9 is a probability distribution from a single test, corresponding to a single point in Fig. 8. This probability histogram is then interpolated to create a smooth surface. The test section in the present work is much shorter than in [49], so the full modal phenomena is not as resolved as the previous work. Nonetheless, the modal transition is clearly observed in these figures, which occurs between 22 and 27 kPa. These plots clearly show that the modal transition occurs at the highest pressure for methane, followed by for ozonated methane, and finally at the lowest pressure for the Boise natural gas. Notably the Boise natural gas has more consistent detonation propagation behavior than high purity methane with and without ozonation. After the modal transition occurs and toward lower pressure, a highly oscillatory velocity is observed. It is difficult to discern any differences among the mixtures tested after the modal transition. A longer test section (similar to that used in [49]) would be required to resolve potential differences, if any.

The data from the two tubes, taken together, lead to a few interesting conclusions. First, the reaction kinetics lead to differences in both limiting behavior and the predictability of the velocity deficit as a function of pressure. This conclusion is most clearly supported by the observation that 3000 PPMv of ozone doping extends the detonation limit (or in the case of the 6.4 mm tube, extends the modal shift point) for high purity methane, and makes detonation propagation more predictable as a function of pressure. The smaller induction length in natural gases than in high purity methane is then presumably responsible for its lower and more predictable detonation limit. In this way, induction length is a reasonable proxy for predicting the detonation limit, at least for mixtures of practically identical thermodynamic conditions.

The second conclusion is that natural gases, despite their relatively wide composition variability, display remarkably narrowly distributed and consistent limiting behavior. This is most clearly observed in Fig. 7b, where the 2σ fast and slow natural gas surrogates display limits close to one another (3.4 kPa vs 4.6 kPa). Furthermore, the Boise natural gas, despite it being a composition outlier (see Tables 1 and 2), exhibits a limit within the bands covered by the natural gas surrogates. In all cases, for both the 32 mm and 6.4 mm ID tubes, the velocity deficit as a function of pressure is much more consistent for natural gases than that for high purity methane. This evidence suggests that using a natural gas in a practical detonation application would lead to a more consistent behavior than using high purity methane, particularly when detonation limiting mechanisms are relevant. On the other hand, using methane as a surrogate for natural gas would predict an erroneously high detonation pressure limit: methane is a less reactive thus highly non-conservative surrogate for natural gas. It is instead recommended that the natural gas surrogates should be used in future studies.

3.4. Geometric limit

To learn more about the nature of the detonation limit, it is informative to plot the velocity limits in normalized coordinates.

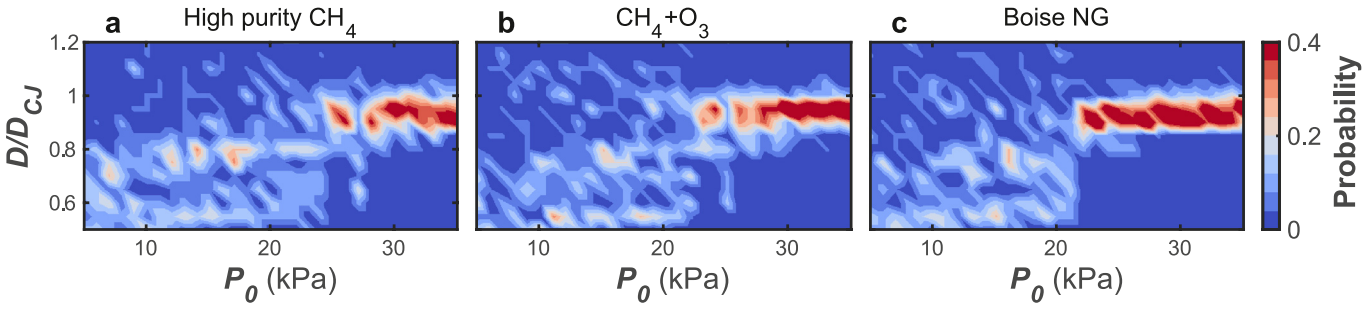

Fig. 9. Normalized local velocity histogram measured as a function of initial pressure in the 6.4 mm ID test section for high purity methane **a**, ozonated methane **b**, and the Boise natural gas **c**.

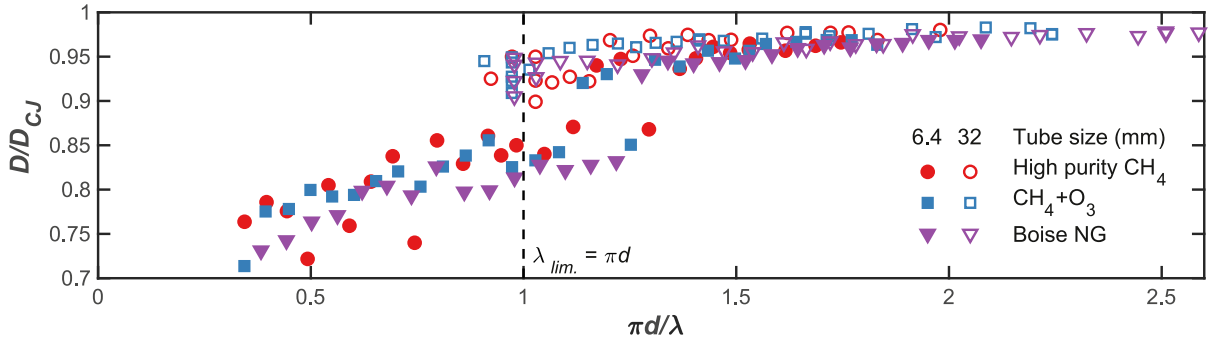

Fig. 10. Normalized velocity as a function of tube perimeter divided by cell width ($\pi d/\lambda$) in both the 6.4 mm ID test section (filled symbols) and 32 mm ID test section (open symbols) for high purity methane (cir cles), ozonated (3000 PPMv) methane (squares), and the Boise natural gas (triangles).

Table 5
Average detonation cell width ($\bar{\lambda}$, mm) and its standard deviation (σ, mm), number of cells measured (n) and calculated ZND induction length (Δ_i, mm) for ozonated methane and the Boise natural gas at several initial pressures and 298 K.

P_0	CH_4 + O_3				Boise NG			
(kPa)	$\bar{\lambda}$	σ	n	Δ_i	$\bar{\lambda}$	σ	n	Δ_i
25	15.5	2.0	13	0.95	11.4	2.1	15	0.81
20	17.2	3.1	10	1.19	13.0	1.5	6	1.00
15	41.2	5.0	6	1.66	18.4	3.2	11	1.33
10	35.1	9.9	7	2.42	39.1	7.0	6	1.99

Namely, the mixture reactivity (as quantified by the detonation cell width) is non-dimensionalized by the tube perimeter, as suggested by Lee et al. [54,55]. To facilitate this non-dimensionalization, the cell width for the ozonated methane and Boise natural gas were measured at several pressures from soot foils. Because a vast experimental dataset already exists for methane at the pressures of interest [56,57], the literature cell size values were used in our analysis. Cursory measurements of methane soot foils yielded similar sizes to those found in the database. The measured average cell widths ($\bar{\lambda}$), their standard deviations (σ), the number of samples taken n, and the calculated induction length (Δ_i) are shown in Table 5. Studies have shown that that induction length correlates linearly, with a constant proportionality constant, with cell size for a given mixture: $\lambda = A\Delta_i$ [33,34,36]. The values for A were determined from literature data for methane, and by averaging the proportionality in Table 5 for the ozonated methane and the Boise natural gas. The values of A thus obtained are $A_{CH_4} = 12.7$, $A_{CH_4+O_3} = 17.4$, and $A_{NG} = 17.5$. These values were used to calculate the cell size for the non-dimensionalization. Note that based on the measured variation in the cell widths the uncertainty in the A values is approximately 25% (no uncertainty was reported in the literature; we assume similar uncertainty to our data).

Figure 10 shows non-dimensionalized velocity, D/D_{CJ}, as a function of the non-dimensionalized reactivity, $\pi d/\lambda$, where πd is the tube perimeter and λ is the detonation cell width. Previous studies showed that the non-dimensionalization leads to a collapse of multiple tube sizes onto a single line for a given mixture [31,54,55]. Although no uncertainty is plotted in this figure for visual simplicity, the uncertainty in the abscissa among different mixtures is approximately 25% due to the uncertainty in the A value, while the uncertainty in the ordinate is less than 2% prior to the modal shift in the 6.4 mm ID tube (and about 10% after the shift). Within the uncertainty of the A values, we observe that the three mixtures and two tube sizes collapse onto a single line. Past observations reported a universal limit at $\lambda_{lim.} = \pi d$, when the tube perimeter is equal to the cell size. In the present study we found the test results in the 32 mm ID tube (open symbols) feature a limit at this point, while the results in the 6.4 mm ID tube (filled symbols) experience the modal shift at around $\pi d/\lambda = 1.15$–1.3. The observation that the modal shift occurs at $\pi d/\lambda \approx 1$ confirms it to be the 'traditional' detonation limit, and any propagation beyond this point is considered a quasi-detonation.

To interpret the difference in behavior between the two tubes tested, the relationship between calculated cell size (using the proportionality constant derived) and initial pressure is plotted in Fig. 11 for each mixture tested. The intersection point between the pressure-cell size relations and the projected limit ($\lambda_{lim.} = \pi d$) for a particular tube corresponds to the predicted limiting pressure for that geometry. Notably, the slope of the pressure-cell size relation lines at the limiting condition (i.e. at the intersection points) is much larger in the 32 mm ID tube than in the 6.4 mm ID tube, for all three mixtures:

$$\left|\frac{d\lambda}{dP_0}\right|_{lim.,d=32\text{mm}} \gg \left|\frac{d\lambda}{dP_0}\right|_{lim.,d=6.4\text{mm}}. \quad (1)$$

It is thus postulated that the difference in these slopes is the cause for the different qualitative limit behavior observed. In the

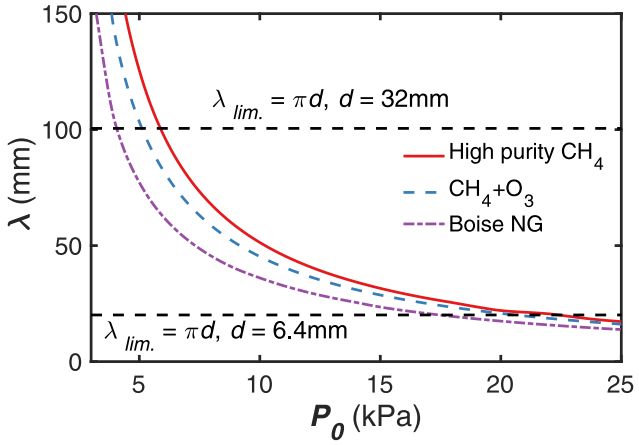

Fig. 11. Calculated cell width (λ) as a function of initial pressure (P_0) for methane (solid line), ozonated methane (dashed line), and the Boise natural gas (dot-dashed line). Expected limits for the two tube sizes considered in this work are plotted as dashed horizontal lines.

case of the 6.4 mm ID tube, when the pressure is lower than the predicted limit pressure, the predicted cell size is still close to the critical cell size, and so small perturbations can cause local deflagration-to-detonation transition (DDT) followed by shock-reaction decoupling. In the 32 mm tube, on the other hand, once the pressure is lower than the limit pressure, the predicted cell size is much smaller than the critical cell size, and so rapid quenching and subsequent total failure occurs.

4. Conclusions

The detonation properties of high purity methane, ozonated (3000 PPMv) methane, an actual natural gas (Boise), and several natural gas surrogates were evaluated using fundamental combustion calculations, ZND simulations, and detonation limit experiments. The main goals of the study were to develop natural gas surrogates, discern the differences in detonation behavior between methane and natural gas, evaluate the sensitivity of detonation to chemical kinetics, and use these results to infer the suitability of using natural gas for detonation applications and to provide insights for safety-related studies. The following conclusions are made:

1. A family of natural gas surrogates were proposed based on the composition variations found in North American natural gases. These surrogates were designed to replicate the mean and variance of fundamental combustion properties of natural gas, and were satisfactorily tested for detonation by comparing the induction lengths computed for the surrogates to the statistical distribution of induction lengths for natural gases of varying compositions. The results suggest that despite their composition variation, North American natural gases have a relatively tight band of detonation behaviors.
2. The expected performance of commercial methane (Grade 1.3 [32]) was compared to that of natural gas using a set of Monte Carlo ZND simulations. It was demonstrated that natural gas is expected to exhibit a limit at a comparatively less reactive condition as compared to the commercial methane. The composition variation of commercial-grade methane is expected to have an impact on detonation predictability similar to North American natural gases. That is, the smaller amounts of minor components and the seemingly small composition variations in commercial-grade methane have nearly the same effect on the detonation property variations as the impurities found in North American natural gas streams.
3. Limit tests were performed in two different tube sizes, a 32 mm ID tube and a 6.4 mm ID tube. In the 32 mm ID tube as pressure decreases for a given mixture a velocity deficit is observed until a critical pressure is reached, below which detonation failure occurred rapidly. In the 6.4 mm ID tube, the same steady velocity deficit is observed as pressure drops, but after a critical pressure is reached, a new mode of quasi-detonation is established which is highly oscillatory. The phenomena is similar for all mixtures tested. Lower critical pressures were observed systematically in all natural gases and in ozonated methane compared to that of high purity methane.
4. The onset of the limit in the 32 mm ID tube and the onset of the modal shift in the 6.4 mm ID tube occurs at the condition where the detonation cell width is equal to or approximately equal to the tube perimeter ($\lambda_{lim.} = \pi d$). The existence of the quasi-detonation in the 6.4 mm ID tube is due to the relatively smaller sensitivity of cell size to initial pressure at the limit.
5. The Boise natural gas and the natural gas surrogates considered in the present study have a substantially smaller induction length than neat methane. Experiments comparing methane and ozonated methane (3000 PPMv) confirm a strong correlation of detonation limits and detonation predictability to induction length. Hence, real natural gases are expected to have more favorable detonation propagation properties (e.g., lower pressure limit) for engine-related applications. In cases where detonation prevention is studied, the current results indicate that natural gases can propagate more readily than methane, and as such methane is in fact a poor surrogate for natural gas.

Declaration of Competing Interest

The authors declare that they have no known competing financial interests or personal relationships that could have appeared to influence the work reported in this paper.

Acknowledgments

This research was funded by the Air Force Office of Scientific Research under Grants FA9550-16-1-0486, FA9550-20-1-0398. JC acknowledges funding from the National Science Foundation Graduate Research Fellowship under Grant DGE-1656518 and the Stanford Graduate Fellowship. The authors also thank Dr. Jiankun Shao and Professor Ron Hanson at Stanford University for providing and measuring the composition of the Boise natural gas sample.

Supplementary material

Supplementary material associated with this article can be found, in the online version, at doi:10.1016/j.combustflame.2021.111719.

References

[1] F.K. Lu, E.M. Braun, Rotating detonation wave propulsion: experimental challenges, modeling, and engine concepts, J. Propul. Power 30 (5) (2014) 1125–1142.
[2] B.A. Rankin, M.L. Fotia, A.G. Naples, C.A. Stevens, J.L. Hoke, T.A. Kaemming, S.W. Theuerkauf, F.R. Schauer, Overview of performance, application, and analysis of rotating detonation engine technologies, J. Propul. Power 33 (1) (2017) 131–143.
[3] V. Anand, E. Gutmark, Rotating detonation combustors and their similarities to rocket instabilities, Prog. Energy Combust. Sci. 73 (2019) 182–234.
[4] D.H. Huang, D.K. Huzel, Modern engineering for design of liquid-propellant rocket engines, American Institute of Aeronautics and Astronautics, 1992.
[5] G.P. Sutton, O. Biblarz, Rocket propulsion elements, John Wiley & Sons, 2016.
[6] M.P. Boyce, Gas turbine engineering handbook, Elsevier, 2011.
[7] S. Frolov, V. Aksenov, V. Ivanov, S. Medvedev, I. Shamshin, N. Yakovlev, I. Kostenko, Rocket engine with continuous detonation combustion of the natural gas–oxygen propellant system, Doklady Physical Chemistry, volume 478, Springer (2018), pp. 31–34.

[8] D.P. Stechmann, S.D. Heister, S.V. Sardeshmukh, High-pressure rotating detonation engine testing and flameholding analysis with hydrogen and natural gas, 55th AIAA Aerospace Sciences Meeting (2017), p. 1931.
[9] J. Kindracki, P. Wolański, Z. Gut, Experimental research on the rotating detonation in gaseous fuels–oxygen mixtures, Shock Waves 21 (2) (2011) 75–84.
[10] C. Welch, D. Depperschmidt, R. Miller, J. Tobias, M. Uddi, A.K. Agrawal, S. Lowe, Experimental analysis of wave propagation in a methane-fueled rotating detonation combustor, ASME Turbo Expo 2018: Turbomachinery Technical Conference and Exposition, American Society of Mechanical Engineers Digital Collection (2018).
[11] I.V. Walters, A. Lemcherfi, R.M. Gejji, S.D. Heister, C.D. Slabaugh, Performance characterization of a natural gas–air rotating detonation engine, J. Propul. Power 37 (2) (2021) 292–304.
[12] C.L. Journell, R.M. Gejji, I.V. Walters, A.I. Lemcherfi, C.D. Slabaugh, J.B. Stout, High-speed diagnostics in a natural gas–air rotating detonation engine, J. Propul. Power 36 (4) (2020) 498–507.
[13] J.M. Mehta, K. Brezinsky, Experimental speciation study of natural gas oxidation using a single pulse shock tube, Int. J. Chem. Kinet. 53 (7) (2021) 845–867.
[14] J. Shao, A.M. Ferris, R. Choudhary, S.J. Cassady, D.F. Davidson, R.K. Hanson, Shock-induced ignition and pyrolysis of high-pressure methane and natural gas mixtures, Combust. Flame 221 (2020) 364–370.
[15] A. Luketa-Hanlin, A review of large-scale LNG spills: experiments and modeling, J. Hazard. Mater. 132 (2–3) (2006) 119–140.
[16] S. Kundu, J. Zanganeh, B. Moghtaderi, A review on understanding explosions from methane–air mixture, J. Loss Prev. Process. Ind. 40 (2016) 507–523.
[17] L. Klebanoff, J. Pratt, C. LaFleur, Comparison of the safety-related physical and combustion properties of liquid hydrogen and liquid natural gas in the context of the sf-breeze high-speed fuel-cell ferry, Int. J. Hydrog. Energy 42 (1) (2017) 757–774.
[18] R. Zipf Jr, V.N. Gamezo, K.M. Mohamed, E.S. Oran, D.A. Kessler, Deflagration–to-detonation transition in natural gas–air mixtures, Combust. Flame 161 (8) (2014) 2165–2176.
[19] R. Zipf Jr, V. Gamezo, M. Sapko, W. Marchewka, K. Mohamed, E. Oran, D. Kessler, E. Weiss, J. Addis, F. Karnack, et al., Methane–air detonation experiments at Niosh lake Lynn laboratory, J. Loss Prev. Process. Ind. 26 (2) (2013) 295–301.
[20] R.K. Zipf, M.J. Sapko, J.F. Brune, Explosion pressure design criteria for new seals in US coal mines, Technical Report, NIOSH, Pittsburgh Research Laboratory, 2007.
[21] V.N. Gamezo, R.K. Zipf Jr, M.J. Sapko, W.P. Marchewka, K.M. Mohamed, E.S. Oran, D.A. Kessler, E.S. Weiss, J.D. Addis, F.A. Karnack, et al., Detonability of natural gas–air mixtures, Combust. Flame 159 (2) (2012) 870–881.
[22] B. Zhang, X. Shen, L. Pang, Y. Gao, Methane–oxygen detonation characteristics near their propagation limits in ducts, Fuel 177 (2016) 1–7.
[23] B. Zhang, H. Liu, B. Yan, H.D. Ng, Experimental study of detonation limits in methane-oxygen mixtures: determining tube scale and initial pressure effects, Fuel 259 (2020) 116220.
[24] D. Kessler, V. Gamezo, E. Oran, Simulations of flame acceleration and deflagration-to-detonation transitions in methane–air systems, Combust. Flame 157 (11) (2010) 2063–2077.
[25] P. Wolański, C. Kauffman, M. Sichel, J. Nicholls, Detonation of methane-air mixtures, Symp. (Int.) Combust. 18 (1) (1981) 1651–1660.
[26] B. Zhang, L. Pang, Y. Gao, Detonation limits in binary fuel blends of methane/hydrogen mixtures, Fuel 168 (2016) 27–33.
[27] M.I. Radulescu, G.J. Sharpe, C.K. Law, J.H. Lee, The hydrodynamic structure of unstable cellular detonations, J. Fluid Mech. 580 (2007) 31–81.
[28] N. Lamoureux, C.-E. Paillard, Natural gas ignition delay times behind reflected shock waves: application to modelling and safety, Shock Waves 13 (1) (2003) 57–68.
[29] Natural gas specs sheet, Technical Report, North American Energy Standards Board, Houston, Texas, Accessed April 2021.
[30] J. Crane, X. Shi, A.V. Singh, Y. Tao, H. Wang, Isolating the effect of induction length on detonation structure: hydrogen–oxygen detonation promoted by ozone, Combust. Flame 200 (2019) 44–52.
[31] X. Shi, J. Crane, H. Wang, Detonation and its limit in small tubes with ozone sensitization, Proc. Combust. Inst. 38 (3) (2021) 3547–3554.
[32] Methane specifications, Technical Report, Praxair, Danbury, Connecticut, Accessed April 2021.
[33] J.H. Lee, The detonation phenomenon, Cambridge University Press, Cambridge, 2008.
[34] C.K. Westbrook, P.A. Urtiew, Chemical kinetic prediction of critical parameters in gaseous detonations, Symp. (Int.) Combust. 19 (1) (1982) 615–623.
[35] C.K. Westbrook, Chemical kinetics of hydrocarbon oxidation in gaseous detonations, Combust. Flame 46 (1982) 191–210.
[36] K.I. Shchelkin, Y.K. Troshin, Gasdynamics of combustion, volume 231, National Aeronautics and Space Administration, 1964.
[37] J. Shao, R.K. Hanson, Boise natural gas gas chromatography, 2019, (personal communication).
[38] G.P. Smith, Y. Zhang, H. Wang, Foundational fuel chemistry model interim version Y (FFCM-Y), 2020, (personal communication).
[39] G.P. Smith, Y. Tao, H. Wang, Foundational fuel chemistry model version 1.0 (FFCM-1), 2016, https://web.stanford.edu/group/haiwanglab/FFCM1/pages/FFCM1.html.
[40] H. Wang, E. Dames, B. Sirjean, D. Sheen, R. Tangko, A. Violi, J. Lai, F. Egolfopoulos, D. Davidson, R. Hanson, et al., A high-temperature chemical kinetic model of n-alkane (up to n-dodecane), cyclohexane, and methyl-, ethyl-, n-propyl and n-butyl-cyclohexane oxidation at high temperatures, 2010. http://web.stanford.edu/group/haiwanglab/JetSurF/JetSurF2.0/index.html.
[41] H.J. Curran, P. Gaffuri, W.J. Pitz, C.K. Westbrook, A comprehensive modeling study of iso-octane oxidation, Combust. Flame 129 (3) (2002) 253–280.
[42] R.J. Kee, F.M. Rupley, J.A. Miller, Chemkin-II: a FORTRAN chemical kinetics package for the analysis of gas-phase chemical kinetics, Technical Report, SAND-89-8009, Sandia National Labs., Livermore, CA (USA), 1989.
[43] A.E. Lutz, R.J. Kee, J.A. Miller, SENKIN: a FORTRAN program for predicting homogeneous gas phase chemical kinetics with sensitivity analysis, Technical Report SAND-87-8248, Sandia National Labs., Livermore, CA (USA), 1988.
[44] P. Glarborg, R.J. Kee, J.F. Grcar, J.A. Miller, PSR: a FORTRAN program for modeling well-stirred reactors, Technical Report SAND86-8209, Sandia National Labs., Livermore, CA (USA), 1986.
[45] R.J. Kee, J.F. Grcar, M.D. Smooke, J.A. Miller, E. Meeks, PREMIX: a FORTRAN program for modeling steady laminar one-dimensional premixed flames, Technical Report SAND85-8249, Sandia National Labs., Livermore, CA (USA), 1985.
[46] S. Browne, J. Ziegler, J. Shepherd, Shock and detonation toolbox, GALCIT-Explosion Dynamics Laboratory, Pasadena, CA, 2008.
[47] D.G. Goodwin, H.K. Moffat, R.L. Speth, Cantera: an object-oriented software toolkit for chemical kinetics, thermodynamics, and transport processes, 2009.
[48] H. Zhao, X. Yang, Y. Ju, Kinetic studies of ozone assisted low temperature oxidation of dimethyl ether in a flow reactor using molecular-beam mass spectrometry, Combust. Flame 173 (2016) 187–194.
[49] S. Jackson, B.J. Lee, J.E. Shepherd, Detonation mode and frequency analysis under high loss conditions for stoichiometric propane-oxygen, Combust. Flame 167 (2016) 24–38.
[50] Y. Gao, H.D. Ng, J.H. Lee, Experimental characterization of galloping detonations in unstable mixtures, Combust. Flame 162 (6) (2015) 2405–2413.
[51] W. Cao, D. Gao, H.D. Ng, J.H. Lee, Experimental investigation of near-limit gaseous detonations in small diameter spiral tubing, Proc. Combust. Inst. 37 (3) (2019) 3555–3563.
[52] V.N. Gamezo, D. Desbordes, E.S. Oran, Formation and evolution of two-dimensional cellular detonations, Combust. Flame 116 (1–2) (1999) 154–165.
[53] B.M. Maxwell, R.R. Bhattacharjee, S.S. Lau-Chapdelaine, S.A. Falle, G.J. Sharpe, M.I. Radulescu, Influence of turbulent fluctuations on detonation propagation, J. Fluid Mech. 818 (2017) 646–696.
[54] J.H. Lee, A. Jesuthasan, H.D. Ng, Near limit behavior of the detonation velocity, Proc. Combust. Inst. 34 (2) (2013) 1957–1963.
[55] Y. Gao, B. Zhang, H.D. Ng, J.H. Lee, An experimental investigation of detonation limits in hydrogen–oxygen–argon mixtures, Int. J. Hydrog. Energy 41 (14) (2016) 6076–6083.
[56] R. Strehlow, Transverse waves in detonations: II. Structure and spacing in H_2-O_2, C_2H_2-O_2, C_2H_4-O_2, and CH_4-O_2 systems, AIAA J. 7 (1969) 492–496.
[57] M. Kaneshige, J.E. Shepherd, Detonation database, Technical Report, 1997.